

Otze – Airborne EM Inversion on Unstructured Model Grids

C. Scholl*
CGG MultiPhysics
Milan, Italy
Carsten.Scholl@cgg.com

F. Miorelli
CGG MultiPhysics
Milan, Italy
Federico.Miorelli@cgg.com

**presenting author asterisked*

SUMMARY

An efficient, accurate, multi-grid algorithm has been implemented for the modeling of airborne, land, and marine controlled source electromagnetic data, providing accurate 3D depth inversions of frequency and time domain data with cost-effective compute timelines. This is achieved by decoupling the inversion grid from the modeling grid used in the finite difference simulation of the fields. The approach helps also when inverting data from different methods jointly.

The model grid consists of columns of prisms that can be arbitrarily dimensioned. This helps to discretize in particular the topography and other interfaces without densely discretizing the upper part of the resistivity model. By setting the horizontal smoothing accordingly, the general geological setting of the survey area can be easily taken into account.

Depending on the specifics of the implementation, other structural information will impact the chosen discretization.

Key words: airborne electromagnetics, multidimensional inversion, x-gradient

INTRODUCTION

The typical AEM data set can consist easily of several thousands of measurement points distributed over large areas. Modelling this data for arbitrary resistivity distributions is computationally demanding and full multidimensional inversions are out of the question. However, several advances in recent years resulted in algorithms that can tackle these problems (Cox and Zhdanov, 2008; Cox et al., 2010, Haber and Schwarzbach, 2014). While the underlying forward solvers use different approaches, the codes make use of the fact that the sensitivity of an AEM system drops off quickly laterally and thus that only a fraction of the total survey area is relevant for a certain measurement point.

Commer and Newman (2006) presented an inversion approach for marine controlled-source EM (mCSEM) data, where the model grid on which the inversion was carried out could be defined independent of the grid used in the finite difference (FD) forward modeling step. The advantage is that the FD grid can be tailored to the specific transmitter-receiver configuration and the frequency or time range that needs to be modelled. For example, higher frequencies required denser grids. Lower frequencies can be modelled using coarser grids, but these need to span larger volumes. The approach was later adopted by Yang et al. (2014) to speed up the inversion of AEM data. And while the survey areas for airborne and marine EM surveys are comparable, the computational savings in the airborne case are much more substantial due to the laterally rapidly decaying sensitivity of AEM systems compared with the typical marine setup.

The downside of the approach is that an additional layer is required during the inversion mapping the model onto the different finite difference grids and conversely sensitivities computed on the FD grid back into model space, which increases the complexity of the code.

Still, when developing the EM inversion code *otze* (starting 2009), the same concept of having a model grid that is not coupled to the FD grid was adopted. However, while the before mentioned studies retained a structured, rectilinear model mesh, we implemented an inversion code that acts on a grid that uses the standard, structured discretization in x and y directions but arbitrary, horizontal interfaces vertically (Scholl and Sinkevich, 2012).

This type of model discretization makes it possible to represent known resistivity interfaces better than standard rectangular meshes without having to go to tetrahedral meshes. In particular, this helps to model topography without having to increase the number of vertical levels throughout the model. Also, this can be used to introduce general knowledge about the stratigraphy in the area into the inverse process.

In this paper we discuss the implementation, its application and show how it can be used to introduce a priori information in the inverse process.

FORWARD MODELLING AND INVERSION

The inversion code acts on 2D or 3D models. Both types of models can be inverted using either a 1D forward algorithm (Weidelt, 2006) or multidimensional solver based on a FD approach. For a 2D model, the latter would be a 2.5D forward solver (Stoyer and

Greenfield, 1976). The 3D solver uses a multigrid preconditioner for efficient simulations (Plessix et al., 2007). Computations are either carried out in frequency domain or in time domain with an implicit time stepping scheme.

Regardless of the dimensionality of the forward solver, the numerical solutions are capable to model arbitrary transmitter/receiver configurations and include system specific details like sensor and transmitter size and shape, current waveforms and primary stripping (Smith, 2001). All solutions were verified for airborne EM (AEM) data by comparison with the code Airbeo (Raiche et al. 2007).

For 3D models, *otze* can also invert magnetic and gravity or gravity gradiometry data, either alone or jointly with EM data. The forward operators for this data is based on the equations presented in Li and Chouteau (1998).

The inversion itself is of the typical regularized least-squares kind that minimizes a cost function of the form

$$\Psi(\mathbf{m}) = (\mathbf{d} - \mathbf{F}(\mathbf{m}))^T \mathbf{W}(\mathbf{d} - \mathbf{F}(\mathbf{m})) + \lambda(\mathbf{m} - \mathbf{m}_0)^T \mathbf{K}(\mathbf{m} - \mathbf{m}_0),$$

where \mathbf{d} is the observed data vector, \mathbf{F} is the forward modeling function, \mathbf{m} is the unknown model vector, \mathbf{W} is a weighting matrix (usually the inverse variance or covariance), λ is the regularization parameter, \mathbf{K} is a discrete form of the stabilizing function as regularization term, and \mathbf{m}_0 is an (optional) a priori model.

Inversion on 2D models is done with an Occam inversion approach (Constable et al., 1987). Inversions on 3D models are done with a preconditioned gradient based method (Rodi and Mackie, 2001). The inversion minimizes the data misfit as well as additional regularization terms. The latter include the commonly employed smoothness constraints and a priori damping as well as other terms which can be used to integrate a priori information, and for lithological classification.

MAPPING OF THE MODEL

One of the key aspects of the inverse program is that the model is decoupled from the meshes used in the forward simulations. In order to carry out the latter, the model has to be mapped onto the finite difference grid.

This happens on the fly using the scheme laid out by Moskow et al. (1999) and Commer and Newman (2006). Note that due to the directionality of the averaging scheme and the different volumes over which the model is averaged, FD elements in different directions (e.g. $\rho_{x,FD}$ and $\rho_{z,FD}$ in Figure 1) typically will get different resistivities, even if the original model is isotropic.

At the air interface, the cells at that boundary are broken up into even smaller pieces during the averaging process. This procedure was found to provide more accurate results than the standard stair-stepping used in more conventional finite difference approaches (Scholl and Sinkevich, 2012).

The inverse process requires the computation of the sensitivities or the gradient, depending on the algorithm. These are computed using the adjoint method (McGillivray et al. 1994). The resulting sensitivities/gradients are properties on the FD grid that have to be mapped back to the model grid.

Yang et al. (2014) use an interpolation method for this mapping. However, we found that this approach resulted in inaccurate sensitivities, in particular once the inversion started to introduce significant structures in the model.

Instead, we employ the chain rule to compute the sensitivity S_{ij} of datum i with respect to the model cells j as

$$S_{ij} = \sum_k S_{ik}^* \frac{\partial \rho_k^*}{\partial \rho_j}$$

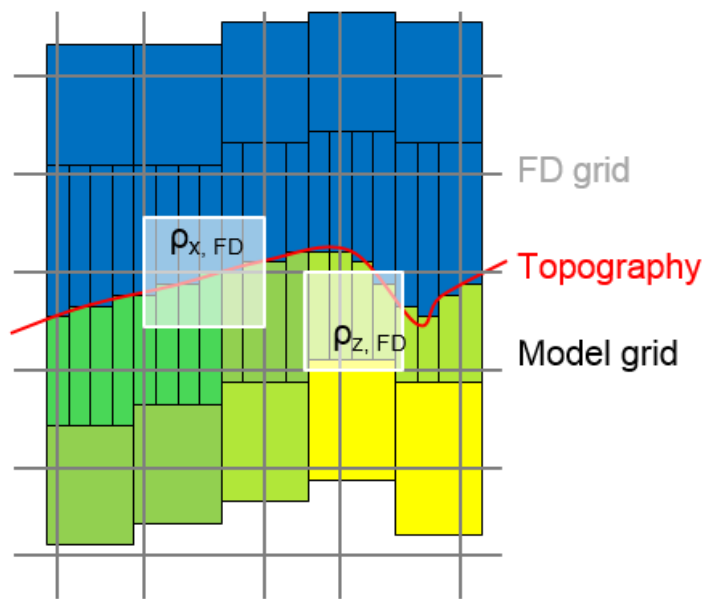


Figure 1: Sketch illustrating how the unstructured model (coloured rectangles; blue boxes represent air) is mapped onto the structured finite difference grid (grey). The white rectangles mark the volumes over which the model has to be averaged for two different elements of the FD grid.

where S_{ij}^* is the sensitivity of datum i w.r.t. the resistivity of FD grid element k and $\partial\rho_k^*/\partial\rho_j$ is the derivative of the resistivity of FD grid element k w.r.t. the resistivity of cell j . The latter is estimated with a simple perturbation scheme. While the time spent on computing the sensitivities this way is not negligible, we found that the convergence of the inversion improves significantly, overall resulting in a reduction of wall-clock time.

The gravity and magnetics forwards are based on solutions for individual prisms. Since their distribution is irrelevant, no complex mapping is required when forward modelling or inverting potential field data.

FIELD DATA EXAMPLES

Time domain (Helitem®) as well as frequency domain data were surveyed by CGG in the Alberta foothills area in Canada, as part of a near-surface characterization program. The upper panel in Figure 2 shows a 2D inversion result using both data sets along one of the flight lines. In this case the model was set up so that it consists of several layers that follow the significant topography while getting thicker with depth. The discretization of the topography is very fine while keeping the overall number of cells low.

The triangles indicate three example positions for the frequency domain (red) and time domain (green) system. The panel in the centre shows vertical resistivities of the FD grids used for the two frequency domain systems; the lowermost panel instead shows the same for the time domain point. The grid spans a larger area but is significantly coarser than the grids for the frequency domain systems which operate at higher frequencies.

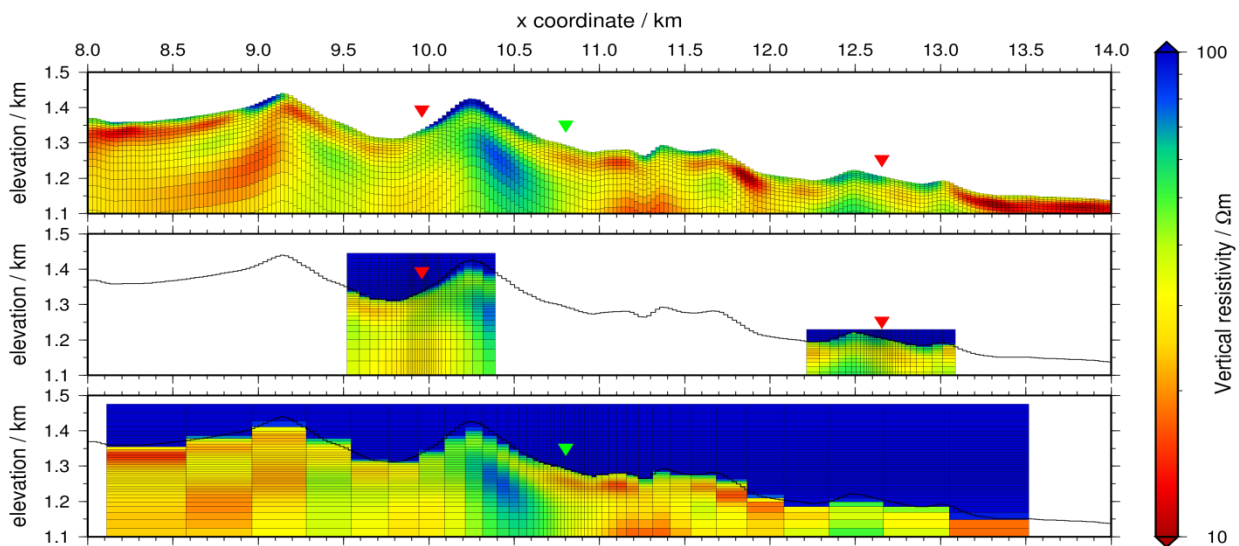


Figure 2: 2D inversion result from a survey in Alberta, Canada (top); FD grid for two measurement points of the frequency domain system (centre); FD grid for one of the time domain points (bottom).

The decoupled model and FD grids allow the user to combine the resolution capabilities of different data sets without caring much about finding computational grids that accurately model both methods simultaneously. An example for the same data set is shown in Figure 3. The uppermost panel shows the inversion result using only the frequency domain system. It provides good resolution at the near surface, but structures start to fade out about 100 m bgl. The panel in the center shows the result of inverting only the time domain data. The structures now extend to greater depths but show less structure in the near surface. The lowermost panel shows the result of a joint inversion of both data sets which retains the near surface structure of the frequency domain result, but also produces deeper reaching dipping structure that matches the known geology in the area (Langenberg and LeDrew, 2001).

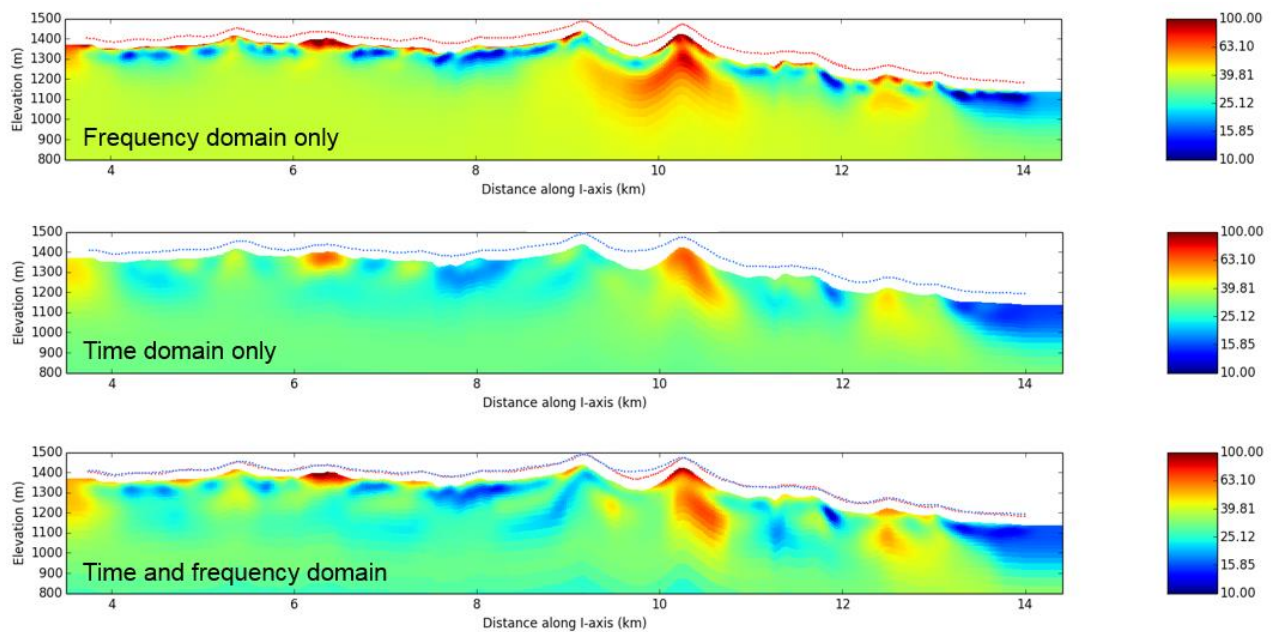


Figure 3: Result of a 2D inversion using only the frequency domain data (top), only the time domain data (centre) and both together in a simultaneous joint inversion (bottom). The dots above the topography indicate the measurement points for the frequency (red) and time (blue) domain system, respectively.

Finally, Figure 4 shows the result of a 3D inversion of time domain data collected with the Helitem35C® system over a mineral deposit in western Tasmania, Australia (Smit et al., 2018). Again, the modelling grid was chosen to follow the topography. Specifically, the figure shows a section and grid level of the model at approximately 80 m bgl. Superimposed on the 3D inversion result is a geobody, partially outlining a known mineral alteration zone which matches the conductive anomaly roughly in the centre of the model.

INCORPORATING STRUCTURAL A PRIORI INFORMATION

While other regularizations are available in *otze*, the most commonly used stabilizer is a smoothness term. Depending on the problem at hand, the smoothing operator can further be modified to include tear surfaces or sharpening elements like Minimum Gradient Support (Zhdanov, 2002) although those are beyond the scope of this paper.

In fact, *otze* uses two separate smoothing terms, one that minimizes the norm of the horizontal gradients, while the other minimizes the vertical resistivity gradients. Depending on the geological environment, these two might be weighted differently w.r.t. each other. For example, in sedimentary settings, the horizontal smoothing will get a larger weight than the vertical smoothing due to the expected layering.

Horizontal smoothing is relatively straightforward with normal, structured grids. With the model discretization used here, however, adjacent cells are not necessarily on the same vertical level. Instead of smoothing a cell strictly to its horizontal neighbours, we chose to connect each cell to only one neighbouring cell; which cell to connect to would be defined by how the model was set up.

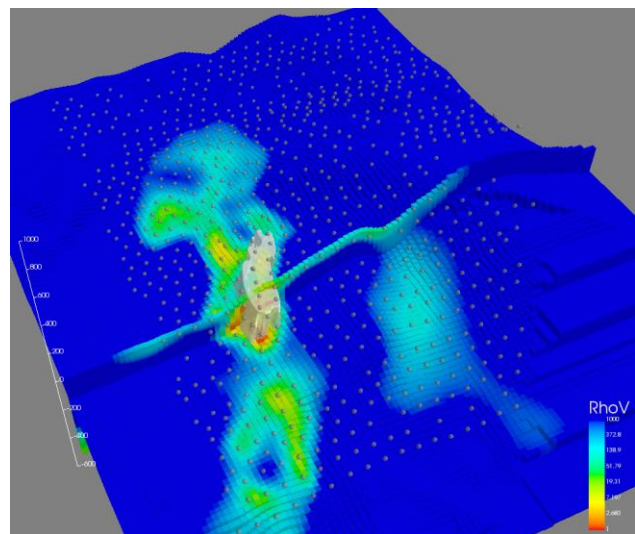
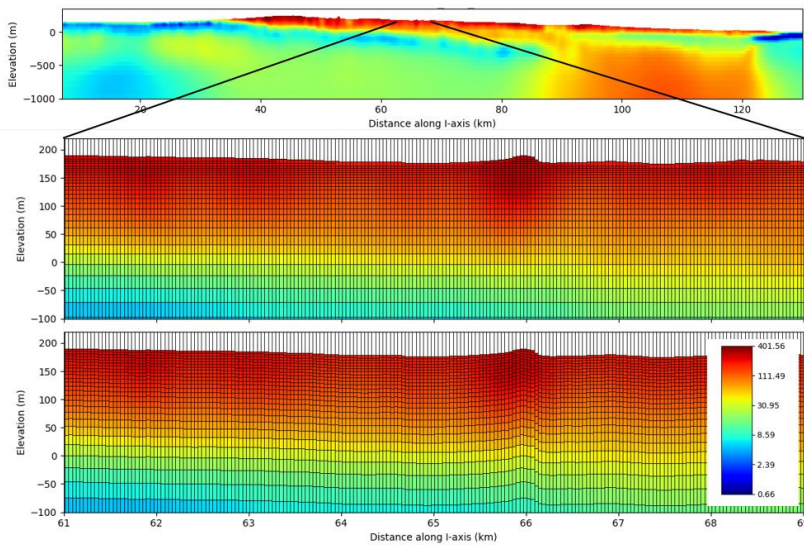


Figure 4: 3D inversion result for a time domain data set collected over a mineral deposit in Tasmania, Australia. The white geobody represents a mineral alteration zone.

Figure 5 illustrates this with an example of a 2D result for data from a time domain data set collected with the TEMPEST system in Australia. The uppermost panel shows the section along the full flight line. The second panel shows a close up of the central part of the upper section. The model in this case shows strictly horizontal layers. As a result, the smoothing operator supports a horizontally layered model as well. This setup would be chosen if the stratigraphy is expected to be mostly horizontal and changes in topography are mostly due to erosion. Note the irregular cells at the air interface to capture the topography, some of which do not have horizontal neighbours. The lowermost panel shows a grid where the layers follow the topography. Likewise, the horizontal smoothing supports features following the topography, which would be useful if the subsurface is supposed to be a folded stack of layers.



Given that the section exhibits only a fairly tame topography, the effect of the change in smoothing is not strong, but still noticeable in the notch below the hill at around 66 km.

Figure 5: 2D inversion result for a fixed wing, time domain survey in Australia. From top to bottom: Complete section, zoom in of a model with strictly horizontal layers, zoom in of a model with layers following the topography.

Another option to include geological a priori information is geosteering (Scholl et al. 2017). Here, an external gradient field that is describing structural features in the area is added to the inversion process via an additional cross-gradient regularisation term (Gallardo and Meju, 2003). This additional term then supports models in which the gradients in the resistivity are either parallel or antiparallel to the given gradient field.

While Scholl et al. (2017) focuses more on the results for some case studies in 2D and 3D, we would like to discuss some details of implementation as the way the gradients are computed in the code is also affected by the potentially arbitrary vertical discretization of the model.

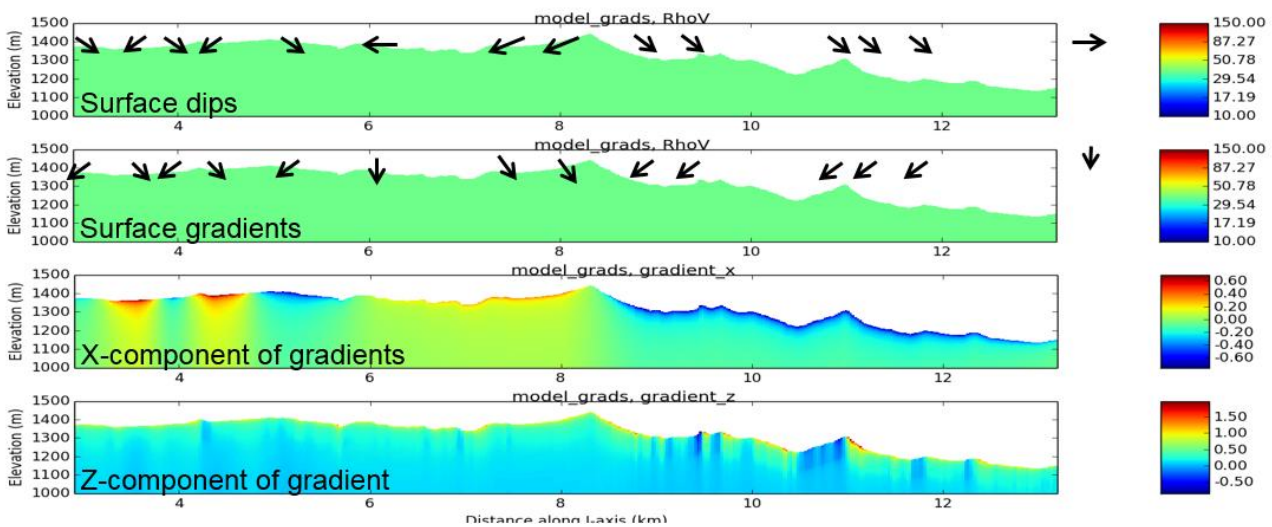


Figure 6: Sketches showing the workflow from surface dips, to gradients to the gradient components as used in the inversion.

As an example of this, Figure 6 shows a few sections, again taken from the dataset from Alberta. The uppermost panel shows a 2D section including some arrows that are supposed to indicate surface dips that have been derived from a geological map (Langenberg and LeDrew, 2001). These dips define planes in which the strata are supposed to stay constant, so the desired gradients which indicate the direction of change are normal to this plane as shown in the second panel.

The vector components are then converted into the correct coordinate system. The result is shown in the lowermost panels. For both components, the magnitude of the components decreases with depth. This reflects that the dips are considered more reliable at the surface but less so at depth.

While the relation between the x-components and the direction of the arrows in the second panel is obvious (the values are negative when the arrows point to the bottom left and positive otherwise), the result for the z-component at first might look confusing as it exhibits strong vertical features. The reason for this is that the gradient components are transformed into the coordinate system of the model. In this case the cell layers follow the topography, so while the vertical base vector points downwards, the one in x-direction points along the topography, i.e. the base is not orthogonal.

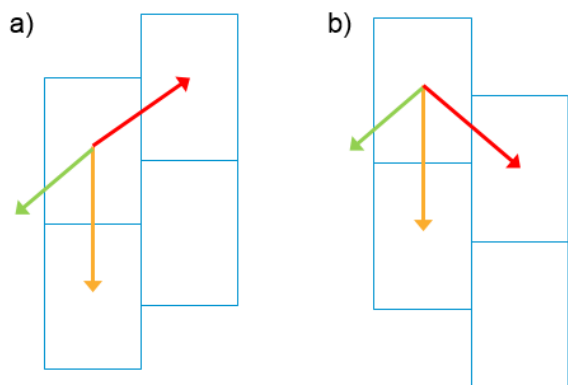


Figure 7: Vertical model base vector (orange) and “x” base vector (red) and surface gradient (green) for a slope going up (a) or down (b) to the right.

Figure 7 shows the situation for the right side of the section: The gradient at the surface points left and down. The model coordinate system is oriented so that x increase to the right. This means that the “x”-component (the one following the slope of the model, red in the figure) needs to be negative in both cases.

In case a), flipping and scaling the red arrow is enough to reproduce the green arrow. The vertical component is not needed and thus zero. In the other case, however, a flipped red arrow – while producing the correct direction horizontally – will go in the upwards, unlike the green arrow. Therefore, a strong contribution from the yellow arrow is needed to fully reconstruct the green arrow.

And this is exactly the pattern that we see in the lowermost section of figure 6: When the elevation increased while going towards the right, the z-component is close to zero, while being larger than 1 otherwise.

The result of including the dips in the inversion is shown in Figure 8 where the section obtained from inversion steered by the surface dips matches the known geology better than the blind inversion without additional information.

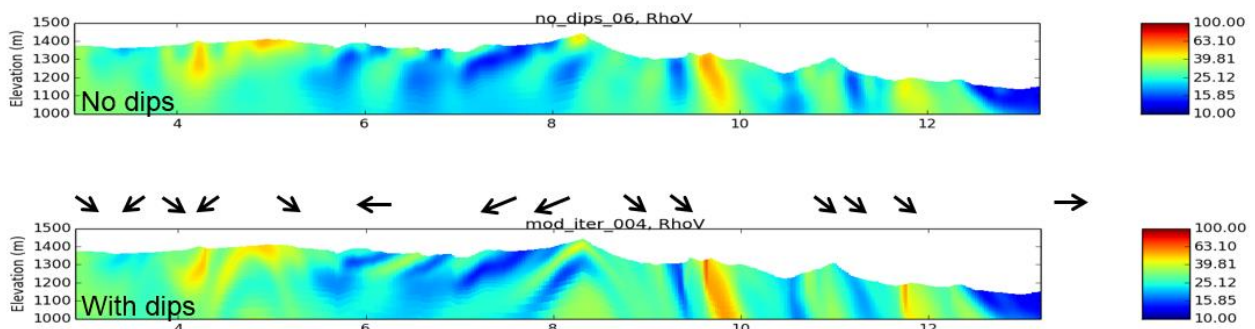


Figure 8: Result of the inversions of time domain data without using surface dips (top) and with using geosteering (bottom).

CONCLUSIONS

Using a vertically unstructured grid helps capture the topography and other features better than standard rectilinear grids without having to add an excessive number of thin layers. The method can also help to introduce stratigraphic information about the survey area in the inversion workflow when setting up the smoothness regularization accordingly.

However, the option to do so by defining which of the cells in the adjacent column is considered its “horizontal” neighbour comes at the price of more bookkeeping in an algorithm that already has an additional layer of complexity due to decoupling the model grid from the computational grids. Furthermore, the specifics of the implementation might have to be taken into account when implementing other geometrical, cell-based regularizations like the x-gradients in the example presented here.

REFERENCES

- Commer M. and G. A. Newman, 2006, New advances in three-dimensional controlled-source electromagnetic inversion, *Geophys. J. Int.*, vol. **172**, 2, 513-535.
- Constable, S.C, R.L. Parker and C.G. Constable, 1987, Occam’s inversion: A practical algorithm for generating smooth models from electromagnetic sounding data, *Geophysics*, **52**, 289-300.
- Cox, L. H., and M. S. Zhdanov, 2008, Advanced computational methods for rapid and rigorous 3D inversion of airborne electromagnetic data: *Communications in Computational Physics*, **3**, 160–179.
- Cox, L. H., G. A. Wilson, and M. S. Zhdanov, 2010, 3D inversion of airborne electromagnetic data using a moving footprint: *Exploration Geophysics*, **41**, 250–259.

- Gallardo, L. A. and Meju, M. A., 2003, Characterization of heterogeneous near-surface materials by joint 2D inversion of dc resistivity and seismic data. *Geophys. Res. Lett.*, **30**, 1658.
- Haber, E. and C. Schwarzbach, 2014, Parallel inversion of large-scale airborne time-domain electromagnetic data with multiple OcTree meshes, *Inverse Problems*, **30**, no. 5.
- Langenberg, C.W., and LeDrew, J., 2001, Geological Map: Coal Valley, NTS Mapsheet 83F/2, 1:50,000 map with cross sections. Alberta Geological Survey Map 237.
- Li, X. and M. Chouteau, M., 1998, Three-Dimensional Gravity Modeling In All Space, *Surveys in Geophysics* **19**: 339. doi:10.1023/A:1006554408567.
- McGillivray, P.R., D.W. Oldenburg, R.G. Ellis and T.M. Habashy, 1994, Calculation of sensitivities for the frequency-domain electromagnetic problem, *Geophys. J. Int.*, **116**, 1-4.
- Moskow, S., V. Druskin, T. Habashy, P. Lee and S. Davydycheva, 1999, A finite difference scheme for elliptic equations with rough coefficients using a cartesian grid nonconforming to interfaces, *SIAM J. Numer. Anal.*, **36**, No. 2, 442-464.
- Plessix, R-E, M. Darnet and W.A. Mulder, 2007, An approach for 3D multisource, multifrequency CSEM modeling, *Geophysics*, **72**, No. 5, SM177-SM184.
- Raiche, A., F. Sugeng and G. Wilson, 2007, Practical 3D EM inversion – P223F software suite: ASEG 19th Geophysical Conference and Exhibition, Perth, Australia.
- Rodi and Mackie, 2001, Nonlinear conjugate gradients algorithm for 2-D magnetotelluric inversion, *Geophysics*, **66**, no. 1, p. 174-187.
- Scholl, C. and V.A. Sinkevich, 2012, Modeling mCSEM data with a finite difference approach and an unstructured model grid in the presence of bathymetry, 21st EM Induction Workshop, Darwin, Australia.
- Scholl, C., S. Hallinan, F. Miorelli, M.D. Watts, 2017, Geological Consistency from Inversions of Geophysical Data, EAGE 2017, Paris, France.
- Smit, J., J. Hooper, A. Smiarowski and C. Scholl, 2018, Mineral Exploration in the Mount Lyell region of Tasmania with the Helitem35C® System, Extended abstract, AEGC2018, Sydney, Australia.
- Stoyer, C.H. and R.J. Greenfield, 1976, Numerical Solutions of the response of a two-dimensional earth to an oscillating magnetic dipole source, *Geophysics*, **41**, 519-530.
- Weidelt, P., 2006, Quasistatic harmonic and transient Fields of electric and magnetic dipoles in a layered Earth: Lecture notes, Institute of Geophysics and Extraterrestrial Physics, Technical University of Braunschweig, Germany.
- Yang, D., D. W. Oldenburg and E. Haber, 2014, 3-D inversion of airborne electromagnetic data parallelized and accelerated by local mesh and adaptive soundings, *Geophys. J. Int.*, vol. **196**, 3, 1492-1507.
- Zhdanov, M.S., 2002, *Geophysical inverse theory and regularization problems*: Elsevier.